A Study of Polyelectrolyte Brushes Formed from Adsorption of Amphiphilic Diblock Copolymers Using the Surface Forces Apparatus

Marc Balastre,[†,§] Feng Li,[†,§] Phillip Schorr,[†] Jinchuan Yang,[‡] Jimmy W. Mays,[‡,⊥] and Matthew V. Tirrell*[,†]

Department of Chemical Engineering and Materials Research Laboratory, University of California at Santa Barbara, Santa Barbara, California 93106, and Department of Chemistry, University of Alabama at Birmingham, Birmingham, Alabama 35294

Received October 29, 2001; Revised Manuscript Received September 30, 2002

ABSTRACT: Polyelectrolyte brushes were formed at the interface between hydrophobized mica and water by adsorbing amphiphilic diblock copolymers consisting of a hydrophobic and a charged block. We measured force−distance profiles with the surface force apparatus (SFA) for several polyelectrolyte brushes of different lengths as a function of aqueous 1:1 electrolyte concentration. Long-ranged electrostatic double-layer forces were not observed in the force curves, and our results suggest that more counterions than predicted by the Manning theory are condensed onto the polymer backbones inside the brush. The brush height observed with the SFA follows the predictions of the mean field theory: at low ionic strength the height is independent of the external salt concentration c_s, whereas at high external ionic strength the height shrinks with a weak power law $L_0 \propto c_s^{-1/3}$. All force vs separation data for three different brushes, with various salt concentrations, collapse with reasonable accuracy into two reduced plots of data in the osmotic and salted brush regimes, respectively, the variables of which are developed in the scope of the mean-field brush theory.

Introduction

Polyelectrolytes remain among the least understood materials in condensed matter science, despite their widespread presence and use. The barrier to understanding is connected with the entwined correlations of chain configurations and charge, coupled with the long-range interactions inherent to these structures. As a natural extension of the study of neutral polymer brushes,[1] end-tethered polyelectrolytes are the central models of many important systems, for example, colloid stabilization[2,3] or lubrication.[4] Polyelectrolyte brushes bring to polyelectrolyte solution physics the additional feature of end-tethering and the resultant confinement to a small surface region. However, this controlled confinement also gives us a well-defined "grip" on one end of every polyelectrolyte chain, thereby giving us a new avenue to study polyelectrolyte chain stretching under the influence on intermolecular interactions, pH, salt, and other controllable parameters of the environment. By studying polyelectrolyte brush model systems, we gain better understanding of the physics of charged macromolecules and are able to provide new ideas for designing biomaterial systems, improving the effectiveness of drug delivery and fine-tuning cell/surface interactions.[5]

Recently, polyelectrolyte brushes have attracted significant attention of theoreticians[6−10] and experimentalists,[11−15] the main challenge being to capture and understand the configurations and forces of interaction in such systems under various conditions. The measurement of brush height, forces between opposing polyelectrolyte layers, and segment density profiles as functions of salt concentration (c_s), adsorption density (σ), number of segments per chain (N), and fraction of free counterions per chain (α) are essential to achieve this aim. A surface forces apparatus (SFA) similar to the design introduced by Israelachvilli et al.[16] was used in this study for the direct force measurements between the opposing polymer layers. This apparatus permits accurate measurements of attractive or repulsive forces, $F(D)$, as a function of the surface separation D. Before presenting the measurements, a brief presentation of some theoretical expectations is given.

Theoretical Considerations

For highly charged and densely tethered polyelectrolyte brushes, the mean-field scaling theories distinguish two different regimes depending on the ionic strength in the solution: the osmotic brush and the salted brush regimes.[9] In the osmotic brush regime, the concentration of counterions inside the brush is greater than the external salt concentration in solution; thus, stretching is produced by the osmotic pressure of the confined counterions.[6] In this regime, the stretching forces are resisted by the elastic force ($F_{el} \cong 3LkT/(Na^2)$), which balance the counterion osmotic pressure ($F_{ion} \cong \alpha NkT/L$), modeled as an ideal gas of counterions:

$$F \cong \frac{3LkT}{Na^2} - \frac{\alpha NkT}{L} \qquad (1)$$

where L is the equilibrium brush height, N is the number of monomer units of Kuhn length a, α is the ratio of the total number of free mobile counterions to the total number of monomer segments, which may be adjusted for counterion condensation,[17] σ is the adsorption density (chains per unit area), and kT is the thermal energy. The balance between the forces leads to the equilibrium thickness of the uncompressed brush L_0:

† University of California at Santa Barbara.
‡ University of Alabama at Birmingham.
§ These authors contributed equally to this work.
⊥ Current address: Department of Chemistry, University of Tennessee, Knoxville, TN 37996.
* To whom correspondence should be addressed: e-mail tirrell@engineering.ucsb.edu.

10.1021/ma011875g CCC: $22.00
Published on Web 11/09/2002

$$L_0 \cong \alpha^{1/2} Na \tag{2}$$

L_0 is expected, by this argument, to be independent of the adsorption density and of the external salt concentration. By integrating eq 1 with respect to L, from L_0 to $D/2$, D being the distance between the two adsorption surfaces, we obtain the interaction free energy G_f per chain.

$$G_f(D) = \int_{L_0}^{D/2} F(L)\, dL \tag{3}$$

which leads to

$$G_f(D) \cong \frac{D^2/4 - {L_0}^2}{Na^2} kT - \alpha NkT \ln\left(\frac{D}{2L_0}\right) = \frac{{L_0}^2 kT}{Na^2}\left[\left(\frac{D}{2L_0}\right)^2 - 1\right] - \alpha NkT \ln\left(\frac{D}{2L_0}\right) \tag{4}$$

Equations 2 and 4 allow us to write the free energy per area, $G_f(D)\sigma$, as a function of $D/2L_0$, where σ represents chains per area:

$$G_f(D)\sigma \cong \sigma\alpha NkTf\left(\frac{D}{2L_0}\right) \tag{5}$$

with $f(D/2L_0) = A_1[(D/2L_0)^2 - 1] - A_2 \ln(D/2L_0)$, A_1 and A_2 being arbitrary constants to account for the fact that there are unknown prefactors in eq 1.

The interaction force measured in the SFA between the two surfaces of crossed cylinder in geometry is normalized by the local geometric mean radius of curvature of the two surfaces, $F(D)/R$. $F(D)/R$ can be related to $G_f(D)\sigma$ by the Derjaguin approximation:[18]

$$\frac{F(D)}{R} = 2\pi G_f(D)\sigma \tag{6}$$

leading to

$$\frac{F(D)}{R} \cong 2\pi\sigma\alpha NkTf\left(\frac{D}{2L_0}\right) \tag{7}$$

When the external salt concentration is greater than the concentration of the counterions inside the brush, the "salted brush" regime is entered. The electrostatic interaction among chain segments becomes screened. The brush remains stretched by the excluded-volume repulsion, where the chains may still be swollen locally (within a Debye length) by electrostatics. This can be modeled using a second virial coefficient. In this "salted regime", the force can be written[6]

$$\frac{F}{kT} \cong \frac{3L}{Na^2} + \omega N \frac{N\sigma}{L^2} \cong \frac{3L}{Na^2} + \frac{\sigma(\alpha N)^2}{c_s L^2} \tag{8}$$

where $\omega \propto \alpha^2/(4c_s)$ is the excluded-volume parameter and c_s is the external salt concentration. The same procedure used for the osmotic regime leads to

$$L_0 \cong \alpha^{2/3} a^{2/3} N\sigma^{1/3} {c_s}^{-1/3} \tag{9}$$

$$\frac{F(D)}{R} \cong \frac{2\pi kT\alpha^{4/3}\sigma^{5/3}N}{a^{2/3}{c_s}^{2/3}}\, g\left(\frac{D}{2L_0}\right) \tag{10}$$

Table 1. Molecular Information and Adsorption Density of PtBS−NaPSS Diblock Copolymers

polymer name	MT3	MT5	MT6
chain length of PtBS block	27	15	15
chain length of NaPPS block, N	747	438	612
degree of sulfonation, β (%)	87	85	84
polydispersity	1.04	1.03	1.04
adsorption density, σ (10^{15} chains/m^2)	7.4 ± 0.2	12.5 ± 0.4	9.5 ± 0.3

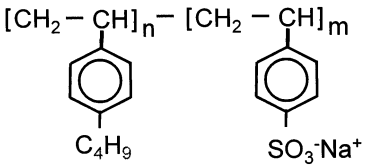

Figure 1. Schematic structure of PtBS−PSSNa.

with a functional form of the force curve given by $g(D/2L_0) = A_3[(D/2L_0)^2 - 1] - A_4[1 - (2L_0/D)]$, A_3 and A_4 being constant prefactors.

Equations 7 and 10 will be tested against experimental data.

Experimental Procedure

In this study, we take the advantage of the amphiphilic nature of hydrophobically modified polyelectrolytes to form the desired brush structure on a hydrophobized mica substrate. A series of various molecular weight diblock copolymers (Table 1), poly(*tert*-butylstyrene)−sodium poly(styrenesulfonate) (PtBS−NaPSS) (Figure 1), were synthesized as described previously.[19] The PtBS block is strongly hydrophobic and insoluble in aqueous media while the NaPSS block is hydrophilic and soluble in water. The diblock copolymers are made highly asymmetric (small PtBS block compared to a large NaPSS block) to ensure water solubility. As indicated in Table 1, the sulfonation levels of the PSS block are around 85%, based on elemental analysis. The hydrophobic PtBS block acts as an anchor toward the surface and adsorbs onto hydrophobic surfaces from aqueous solutions.

Normal Force Measurements. Force measurements were carried out on a surface forces apparatus (SFA) similar to the Israelachvili design.[16] The basic techniques[20] and the detailed experimental procedures involved in force measurements have been described elsewhere.[21] In a typical experiment, two mica pieces were glued onto the two cylindrical lenses. Monolayers of octadecyltriethoxysilane (OTE) were transferred by a Langmuir−Blodgett technique onto mica substrates that had been treated with water plasma to generate hydroxyl groups on the surface. The details of this mica surface modification are described in the next paragraph and discussed elsewhere.[22] After deposition of the OTE layer, the two lenses were mounted in the SFA and a thickness of 20 ± 5 Å for the OTE layer was measured. This result is in accordance with the literature.[23,24] The SFA was then filled with a solution of 80 ppm PtBS−PSSNa in 0.3 M $NaNO_3$, a salt which was found to produce less deterioration over long periods of time of the silvered mica surfaces of the SFA than NaCl and is high enough in concentration to produce a significant adsorbed amount[19] (see Table 1). This polymer concentration exceeds the critical micelle concentration of the block copolymers used.[25]

Once filled, the two surfaces were separated to approximately 1 mm. After 14 h, the solution was replaced with pure water to quench the adsorption. $NaNO_3$ solution was added into the box until the concentration reached about 0.3 M. A force−distance profile (F/R vs D) was obtained at this concentration, where R is the mean curvature of the cross-cylindrical lenses. The bulk salt concentration was then gradually diluted, and force−distance profiles at different salt concentrations were measured. The salt concentration in the bulk solution was measured with a conductivity probe. All adsorption and force measurement experiments were done at temperatures of $T = 30 \pm 0.2$ °C. No desorption was observed during the

experiment, in good agreement with our adsorption experiments by using ellipsometry, which also show no desorption at similar conditions.[19,25] After the compression/separation cycles at the lowest salt concentration, 0.3 M $NaNO_3$ was again introduced, and the force measurement was repeated; the same force curves as originally measured at 0.3 M were obtained.

Hydrophobic Surface Preparation. Langmuir−Blodgett (LB) deposition were carried out using a KSV 5000 Langmuir trough. LB monolayers were deposited onto cylindrically curved glass lenses with a 1 cm^2 mica coupon (thickness 2−3 μm) glued to them. The lenses were held by stainless steel tweezers for the deposition. The protocol developed by Wood and Sharma[23] was slightly modified. Monolayers of OTE were transferred onto mica surface that had been treated with argon/water-vapor plasma (30 min at 20 W). The water vapor flow rate was such that the pressure in the plasma chamber (initially at 34 mT) was maintained at 54 mT. Transfer of the OTE monolayer was performed at 30 mN m^{-1}. 35 μL of OTE solution was spread from a 2 mg/mL OTE solution in chloroform/methanol (95/5), onto a subphase of neutral pH, and allowed to stand for 30 min before compressing the film to 30 mN m^{-1} at a rate of 10 mm/s. The pH of the subphase was then lowered to pH 2 ± 0.5 using sulfuric acid, and the film was allowed to stand compressed at 30 mN m^{-1} for 90 min. Deposition of the monolayer was performed at 1 mm/min with a transfer ratio of 0.95 ± 0.05. After drying in a clean air stream for 15 min, these samples were annealed at 100 °C for 120 min. This protocol produced relatively smooth and homogeneous OTE surfaces on mica.[22] Any small scale roughness that was produced on the surface was irrelevant at the length scales of the polyelectrolyte force measurements. The resulting contact angle of the hydrophobic OTE layer was about 110°, in accord with other studies.[23,24]

Adsorption Density Measurements. Using ellipsometry, we measure separately the adsorbed amount on an OTE-covered SiO_2 substrate. The OTE deposition was carried out using a simpler method than that described in the previous section,[24] leading to the same water contact angle. Therefore, we assume the two OTE surfaces to be equivalent in terms of the amounts of adsorbed polymer; we, therefore, calculated the adsorption density under the same adsorption conditions from the ellipsometric measurements.[26] The average value of σ obtained in this way, reported in Table 1, exceeds the overlap concentration for chains on the surface. We know that there is some heterogeneity of adsorption of the hydrophobic block,[14] as seen in atomic force microscopy images, but this heterogeneity is at a much smaller scale than that of the contact region over which the SFA measurement is made. These surfaces are homogeneous from the point of view of ellipsometry and SFA.

Results

Figures 2−4 show the force profiles of three NaPSS brushes with different molecular weights (MT6, MT5, and MT3, respectively) in water of various salt concentrations. The forces were measured with the surfaces both approaching and retreating from each other. At each particular salt concentration, the compression curves overlap the separation curves very well, indicating that no appreciable hysteresis is observed in any of these experiments. The superposition of compression and separation curves is good evidence that possible effects of weak adsorption of PSS on the hydrophobic surface are negligible. This contrasts with many observations of hysteresis in SFA measurements between adsorbed polyelectrolyte layers.[27,28] The measured interaction forces are purely repulsive for both compression and separation. The force profiles clearly show the influence of the external salt on the conformation of the adsorbed polyelectrolyte chains.

Several features are evident from visual observation of the data and identical for all the brushes described in Figures 2−4. Figure 4, for example, is a convenient

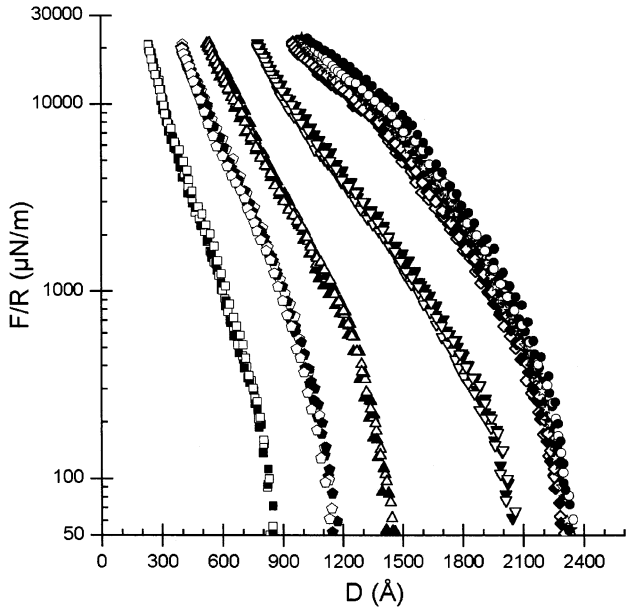

Figure 2. Normalized force−distance profiles of $PtBS_{15}$/$NaPSS_{612}$ (MT6) at different added salt ($NaNO_3$) concentration: 0.30 M (square), 0.12 M (pentagon), 0.056 M (triangle up), 0.020 M (triangle down), 5.4 mM (diamond), 0.92 mM (star), and 0.11 mM (circle). Filled symbols refer to compression force curves, and open symbols refer to separation force curves. Force curves of several compression/separation cycles are presented at each salt concentration.

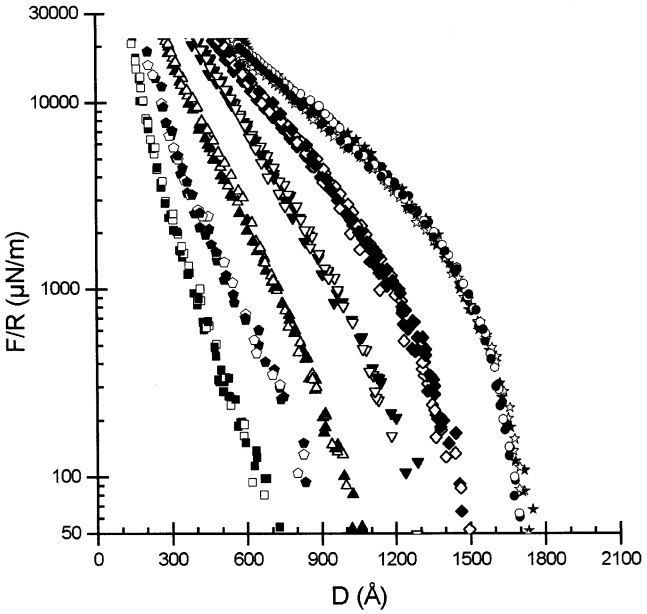

Figure 3. Normalized force−distance profiles of $PtBS_{15}$/$NaPSS_{438}$ (MT5) at different added salt ($NaNO_3$) concentration: 0.30 M (square), 0.16 M (pentagon), 0.076 M (triangle up), 0.034 M (triangle down), 0.012 M (diamond), 0.91 mM (star), and 0.15 mM (circle). Filled symbols refer to compression force curves, and open symbols refer to separation force curves. Force curves of several compression/separation cycles are presented at each salt concentration.

place to discuss these features. On reducing the concentration of $NaNO_3$ from 0.49 to 9.1×10^{-5} M, two regimes of behavior were observed. In the first regime, from 0.49 to 0.020 M $NaNO_3$, the interaction range shifts progressively to larger distance. This decrease of the ionic strength leads to decrease of the screening and increase of electrostatic excluded-volume repulsion, which gives rise to the expansion of the "salted" brush.

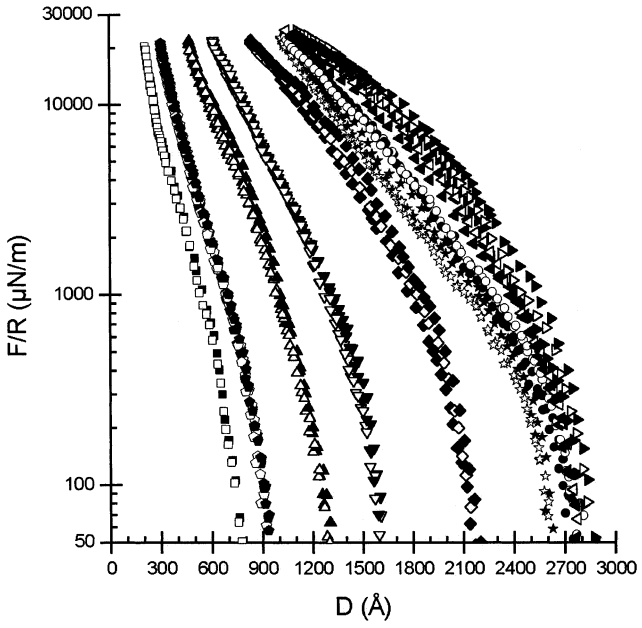

Figure 4. Normalized force−distance profiles of $PtBS_{27}$/$NaPSS_{747}$ (MT3) at different added salt ($NaNO_3$) concentration: 0.49 M (square), 0.30 M (pentagon), 0.12 M (triangle up), 0.052 M (triangle down), 0.020 M (diamond), 9.2 mM (star), 2.8 mM (circle), 0.57 mM (triangle left), and 0.091 mM (triangle right). Filled symbols refer to compression force curves, and open symbols refer to separation force curves. Force curves of several compression/separation cycles are presented at each salt concentration.

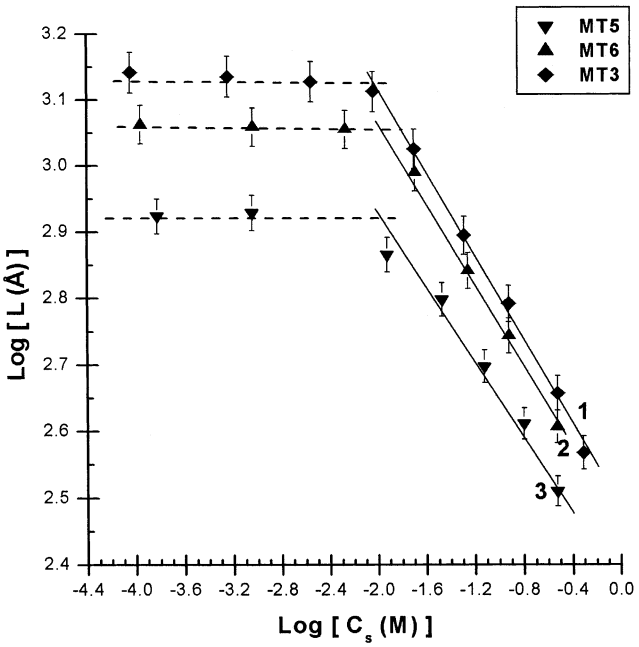

Figure 5. Salt concentration dependence of the brush height for the three different brushes. The solid and dashed lines are linear fits. The dashed lines have slopes close to zero. The slopes for the linear fit 1, 2, and 3 are -0.33 ± 0.02, -0.33 ± 0.02, and -0.30 ± 0.02, respectively.

In a second regime ("osmotic brush" regime), observed here at lower salt concentrations of $0.0092-9.1 \times 10^{-5}$ M, the force curves almost remain the same, which suggests that not only the brush height but also the segment distribution has a very weak dependence on the external salt concentration.

Interestingly, the force curves become softer (less abrupt increase of force at smaller separations) with decreasing salt concentration, meaning that the segment distribution is becoming more diffuse. This agrees with theoretical analysis[8] and other experimental observations.[12] The force profiles of other molecular weights (Figures 2 and 3) show very similar behavior.

Discussion

When two polyelectrolyte brush layers are brought together, a steric repulsive force develops when the segments of the two opposing layers come into contact with each other. Furthermore, a longer-ranged electrical double-layer force might also be observed if the counterion clouds of the two layers come into to overlap before steric interactions occur.[15,29] However, most theories of polyelectrolyte brushes[6,9,10,30] assume that all of the counterions are trapped inside the polyelectrolyte brush. Under this assumption of brush electroneutrality, the counterion cloud extends only negligibly outside the brush; thus, the long-ranged electrical double-layer force does not exist. Indeed, none of the measured force curves in Figures 2−4 exhibit the exponential tail of the electrostatic double-layer force at any salt concentration, which indicates that the long-ranged electrostatic interaction was not observed.[31] The onset of the measured force can be regarded as the interaction range of the steric forces. Thus, the separation distance at which the interaction forces are first detectable equals twice the brush height ($2L_0$). Hence, the brush height can be estimated at each salt concentration for each polymer. The absence of the electrostatic tail is also a strong indication that the low salt data actually are in the osmotic brush regime.

To examine the scaling relationship between brush height and salt concentration for different brushes, a log−log plot (log L_0 vs log [$NaNO_3$]) was constructed for MT3, MT5, and MT6. As shown in Figure 5, one can easily distinguish the osmotic brush and salted brush regime. For each molecular weight, the brush height L_0 is nearly constant and independent of the bulk salt concentration in the osmotic brush regime at low c_s. While in the salted brush regime, the brush height shrinks upon the addition of monovalent counterions, and the slopes of the three different brushes are all very close to $-1/3$, which is in good agreement with the scaling law[9] $L_0 \propto c_s^{-1/3}$. The overlap of the data for different molecular weights in both regimes is consistent with the linear scaling of L_0 with N, embodied in eqs 2 and 9.

The transition from the osmotic brush to the salted brush happens when the bulk salt concentration equals the free mobile counterion concentration. We determine the crossover concentration c_0 from Figure 6, which turns out to be in the range from 0.01 to 0.02 M for the three different brushes. The Debye screening length κ^{-1} and Gouy−Chapman length Λ at the crossover concentration can be calculated by using $\kappa^{-1} = (8\pi l_B c_0)^{-1/2}$ and $\Lambda = (2\pi l_B c_0 L_0)^{-1}$, where l_B is the Bjerrum length (7.14 Å for water).[18] The Gouy−Chapman length is defined as the characteristic thickness of the counterion cloud near a charged surface.[32] As in Table 2, both κ^{-1} and Λ are much smaller than the brush height L_0. Therefore, the decay of the counterion density from a mean value of $N\alpha/L_0$ inside the brush, to zero in the external solution, occurs within a narrow region of thickness κ^{-1} at the brush/solution interface ($\kappa^{-1} \ll L_0$, 30 Å vs 1300 Å in the case of MT3). This explains why no electrical double-layer force is observed in the force profiles.

Table 2. Debye Screening Length and Counterion Condensation

polymer name	MT3	MT5	MT6
crossover concentration, c_0 (M)	0.011 ± 0.002	0.015 ± 0.002	0.013 ± 0.002
Debye screening length at c_0 (Å)	29 ± 2	25 ± 2	27 ± 2
Gouy−Chapman length at c_0 (Å)	2	3	3
maximum height of the brush (in % of the contour length)	71 ± 5	79 ± 5	75 ± 5
concentration of free counterions inside the brush (M)	0.011 ± 0.002	0.015 ± 0.002	0.013 ± 0.002
concentration of total counterions inside the brush (M)	0.059 ± 0.002	0.091 ± 0.002	0.071 ± 0.002
fraction of counterion condensation (%) (experimental)	81 ± 5	84 ± 5	82 ± 5
fraction of counterion condensation by the Manning theory (%)	60	59	58

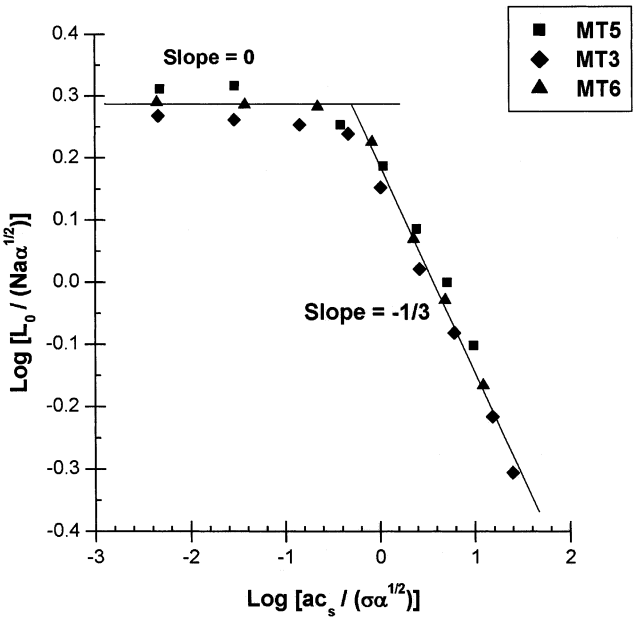

Figure 6. A master curve for the brush height. The brush height L is a function of N, α, σ, and c_s for salted brush and only depends on N and α for the osmotic brush. The solid lines (with slopes of $-1/3$ and 0, respectively) are the theoretically expected power laws for the salted brush and osmotic brush, respectively.

The total counterion concentration inside the brush, including both free counterions and condensed counterions, can be calculated assuming that all the counterions remain inside the brush, through $c_T = \beta\sigma N/(L_c N_{av})$, where β is the degree of sulfonation of the polyelectrolyte chains, L_c refers to the brush height at the crossover, and N_{av} is Avogadro's number. Condensation here means close association of a counterion with a polyelectrolyte chain. The transition between the salted regime and osmotic brush regime is defined as the point where the osmotic pressure from the salt ions in solution outside the brush equals the osmotic pressure from the salt ions inside the brush. Since only the fraction of counterions that are uncondensed contribute to the osmotic pressure, we assume that the free counterions trapped in the brush equal the crossover concentration. Therefore, the resulting fraction of condensed counterions reported for different molecular weights in Table 2 suggests that in all cases about 80% of the counterions inside the brush are condensed.

This observation implies that the majority of counterions is bound to the polyelectrolyte chains and that the fraction of counterion condensation is higher than the value predicted by the Manning theory (Table 2). The fraction of counterion condensation predicted by the Manning theory[17] equals $1 - b/l_B$, where b is the average contour length between two neighboring monomers. Since the polymer chains are not 100% charged, $b = 2.5$ Å$/\beta$. This fraction of counterion condensation is in close agreement with another experimental study on a quenched polyelectrolyte brush studied by X-ray reflectivity.[13] This result indicates that the actual counterion condensation amount for brushes exceeds the value predicted by the Manning theory by about 20−25%. The origin of this difference is not certain. A possible explanation for this is that, due to the overlap of the polyelectrolyte chains in the brush structure, for a selected charged monomer, the closest charged monomer may not be on the same chain but on a neighboring backbone, and this on average leads to a decrease in the contour length b.

For polyelectolyte brushes, our data support the predictions of simple models which predict that the brush height scales with molecular weight to the first power for both salted and osmotic brush regimes. This stronger dependence on molecular weight implies that the tethered chains are highly stretched as compared to the untethered case. Table 2 shows that when the brushes are maximally stretched, a value of about 70−80% of the contour length is reached. Even though the adsorption densities of these polyelectrolyte brushes are lower than those of many neutral polymer brush constructions studied in our laboratory and others,[34] the stretching here is much greater than has been observed in neutral brushes.

According to the predictions of eqs 2 and 9, the brush height depends on four variables: the chain length N, fraction of free counterions α, adsorption density σ, and salt concentration c_s. It is desirable to plot all our data in a master curve based on the scaling forms of eqs 2 and 9, which takes all four parameters into consideration. Here, α is the charge density after counterion condensation and is calculated from the data in Tables 1 and 2; i.e., $\alpha = \beta^*(1-81\%) = 0.17$ for MT3 and β is 87% here. In Figure 6, $L_0/(Na\alpha^{1/2})$ is plotted vs $ac_s/(\sigma\alpha^{1/2})$, and all the data fall onto a universal curve in a log/log plot, which has a slope of zero in the low salt regime and a slope of $-1/3$ in the high salt regime. This supports the validity of the asymptotic relations $L_0 \propto \alpha^{1/2}Na$, for osmotic brush, and $L_0 \propto \alpha^{2/3}N\sigma^{1/3}c_s^{-1/3}$, for salted brush.

Figures 7 and 8 show the plots of $(F/R)/(2\pi kT\sigma\alpha N)$ vs $D/2L_0$ and $(F/R)a^{2/3}C_s^{2/3}/(2\pi kT\sigma^{5/3}\alpha^{4/3}N)$ vs $D/2L_0$, as suggested by eqs 7 and 10, respectively, for the three different molecular weights in the osmotic regime and the salted regime. In each regime, all the force profiles collapse without any adjustable parameters, indicating that the physics of our system is well described by eqs 7 and 10 and therefore by the simple force balances embodied in eqs 1 and 8. The two universal force curves in Figures 7 and 8 can be fit reasonably well by the two equations $f(x) = A_1(x^2 - 1) - A_2 \ln(x)$ and $g(x) = A_3(x^2 - 1) - A_4[1 - (1/x)]$, respectively. The constants are $A_1 = 0.75$, $A_2 = 1.62$, $A_3 = 0.45$, and $A_4 = 1.01$. The ratios A_2/A_1 and A_4/A_3 are both 2.2, indicating the osmotic repulsion dominates the elastic force in both brush regimes.

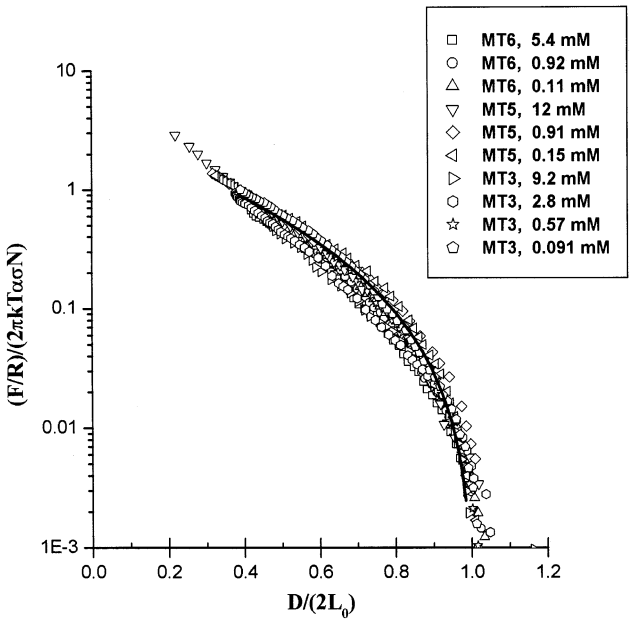

Figure 7. A universal curve of force profiles in the osmotic brush regime, incorporating data for the three different molecular weights. One force curve is shown for each salt concentration. The separation is been normalized by twice of the equilibrium brush height at the corresponding salt concentration, and the measure force F/R is normalized by the prefactor ($2\pi kT\sigma\alpha N$), which is derived from the scaling theory. The solid line is a fit by using the function $f(x) = A_1(x^2 - 1) - A_2 \ln x$ (with $x = D/2L_0$) where $A_1 = 0.75$ and $A_2 = 1.62$.

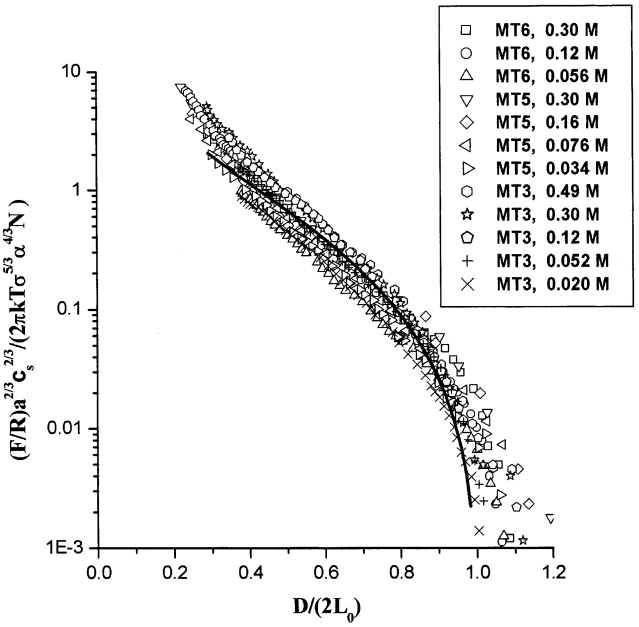

Figure 8. A universal curve of force profiles in the salted brush regime, incorporating data for the three different molecular weights. One curve is shown for each salt concentration. The separation is been normalized by twice of the equilibrium brush height at the corresponding salt concentration, and the measure force F/R is multiplied by the prefactor $a^{2/3}C_s^{2/3}/(2\pi kT\sigma^{5/3}\alpha^{4/3}N)$, which is derived from the scaling theory. The solid line is a fit by using the function $g(x) = A_3(x^2 - 1) - A_4(1 - 1/x)$ (with $x = D/2L_0$) where $A_3 = 0.45$ and $A_4 = 1.01$.

In comparing Figures 7 and 8, it is interesting to note that, in the regions of weaker compression ($D/2L_0$ value greater than 0.4), the universal force curves in the osmotic regime and salted regime can overlap each other well. Differences between the two regimes start to occur for higher compression ($D/2L_0$ value lower than 0.4), where it appears that there is more resistance to compression of the two layers in the salted regime than in the osmotic regime. This divergence is not suggested by the scaling model, because the concentration of the free counterions inside a salted brush increases with compression, and it will exceed the bulk salt concentration and become indistinguishable from an osmotic brush at sufficient high compression. Therefore, the theory, which explains most features of our data quite well, does not offer an explanation for the divergence of the normalized force data in the two regimes at high compression. Overall, however, we feel the simple models tested here perform very well.

Conclusion

We have performed direct force measurement on three quenched polyelectrolyte (PtBS−NaPSS) brush systems at various bulk salt concentrations. The measured forces can be regarded as the contributions of steric interactions and short-ranged electrostatic interactions. Long-ranged electrostatic double-layer forces have not been detected. A large fraction of counterions condenses onto the polyelectrolyte backbones, while the rest of the counterions are trapped inside the brush. Finally, we successfully assembled all our data into a "universal brush height curve", which considers all factors that affect the brush height. A "universal force profile" was successfully drawn in each brush regime (osmotic and salted), based on equations derived from the scaling theory. All our results clearly demonstrate the validity of the scaling theory for both osmotic brush and salted brush regimes and give an idea of the contribution of the different forces at play in each case.

Acknowledgment. We are very grateful to E. Hernandez-Zapata, M. N. Tamashiro from P. Pincus' group, Ryan Toomey, and Markus Biesalski for helpful discussions. This work was financially supported by NSF Grant CTS-9616797 from the CTS and DMR Divisions of the National Science Foundation and partially by the MRL program of the National Science Foundation under Award DMR00-80034 and the Institut Français du Pétrole (I.F.P., France).

References and Notes

(1) Milner, S. T. *Science* **1991**, *251*, 905.
(2) Goodwin, J., Ed. *Colloidal Dispersions*; Royal Society of Chemistry: London, 1982.
(3) Dautzenberg, H.; Jaeger. W.; Kötz, J.; Philipp, B.; Seidel, Ch.; Stscherbina, D. *Polyelectrolytes: Formation, Characterization and Applications*; Hanser: New York, 1994.
(4) Klein, J.; Kamiyama, Y.; Yoshizawa, H.; Israelachvili, J. N.; Fredrickson, G. H.; Pincus, P.; Fetters, L. J. *Macromolecules* **1993**, *26*, 5552.
(5) Hammer, D.; Tirrell, M. *Annu. Rev. Mater. Sci.* **1996**, *26*, 651.
(6) Pincus, P. *Macromolecules* **1991**, *24*, 2912.
(7) Misra, S.; Varanasi, S.; Varanasi, P. *Macromolecules* **1989**, *22*, 4173.
(8) Tamashiro, M. N.; Hernandez-Zapata, E.; Schorr, P.; Balastre, M.; Tirrell, M.; Pincus, P. *J. Chem. Phys.* **2001**, *115*, 4.
(9) Borisov, O. V.; Zhulina, E. B.; Birshtein, T. M. *Macromolecules* **1994**, *27*, 4795.
(10) Israels, R.; Leermakers, F. A. M.; Fleer, G. J.; Zhulina, E. B. *Macromolecules* **1994**, *27*, 3249.
(11) Guenoun, P.; Schlachi, A.; Sentenac, D.; Mays, J. W.; Benattar, J. *Phys. Rev. Lett.* **1995**, *74*, 3628.
(12) (a) Mir, Y.; Auroy, P.; Auvray, L. *Phys. Rev. Lett.* **1995**, *75*, 2863. (b) Tran, Y.; Auroy, P.; Lee, L.-T. *Macromolecules* **1999**, *32*, 8952.
(13) Ahrens, H.; Förster, S.; Helm, C. A. *Phys. Rev. Lett.* **1998**, *81*, 4172.

(14) Kelley, T. W.; Schorr, P. A.; Johnson, K. D.; Tirrell, M.; Frisbie, C. D. *Macromolecules* **1998**, *31*, 4297.
(15) Abraham, T.; Giasson, S.; Gohy, J. F.; Jérôme, R. *Langmuir* **2000**, *16*, 4286.
(16) (a) Israelachivilli, J. N.; Tabor, D. *Proc. R. Soc. London* **1972**, *A331*, 19. (b) Israelachivilli, J. N.; Adams, G. E. *J. Chem. Soc., Faraday Trans.* **1978**, *174*, 975.
(17) Manning, G. S. *J. Chem. Phys.* **1969**, *51*, 924.
(18) Israelachivilli, J. N. *Intermolecular and Surface Forces*; Academic Press: London, 1992.
(19) Zhang, Y.; Tirrell, M.; Mays, J. W. *Macromolecules* **1996**, *29*, 22, 7299.
(20) Israelachvili, J. N. *Acc. Chem. Res.* **1987**, *20*, 415.
(21) Hadziioannou, G.; Patel, S.; Granick, S.; Tirrell, M. *J. Am. Chem. Soc.* **1986**, *108*, 2869.
(22) Li, F.; Balastre, M.; Schorr, P.; Tirrell, M., to be published.
(23) Wood, J.; Sharma, R. *Langmuir* **1994**, *10*, 2307.
(24) Peanasky, J.; Schneider, H. M.; Granick, S.; Kessel, K. *Langmuir* **1995**, *11*, 953.
(25) Toomey, R. Ph.D. Thesis, University of Minnesota, 2001.
(26) Zhang, Y. Ph.D. Thesis, University of Minnesota, 1996.
(27) Luckham, P.; Klein, J. *J. Chem. Soc., Faraday Trans. 1* **1984**, *80*, 865.
(28) Watanabe, H.; Patel S. S.; Argillier, J. F.; Parsonage, E. E.; Mays, J.; Dan-Brandon, N.; Tirrell, M. *Mater. Res. Soc. Symp. Proc.* **1992**, *249*, 255.
(29) Abe, T.; Higashu, N.; Niwa, M.; Kurihara, K. *Langmuir* **1999**, *15*, 7725.
(30) Misra, S.; Tirrell, M.; Mattice, W. *Macromolecules* **1996**, *29*, 6056.
(31) If the tails are due to the electrical double-layer force, the slopes of linear tails in the semilog plots (Figure 2−4) should be proportional to the inverse of Debye screening length. Therefore, the slopes should be a linear function of $c_s^{1/2}$. However, such linear relationship does not exist. We also could not fit the curves with DLVO treatment following the recipe of Chan et al.[33]
(32) Evans, F.; Wennerström, H. *The Colloidal Domain: Where Physics, Biology, and Technology Meet*; VCH: Weinheim, 1994.
(33) Chan, D. Y.; Pashley, R. M.; White, L. R. *J. Colloid Interface Sci.* **1980**, *77*, 283.
(34) Watanabe, H.; Tirrell, M. *Macromolecules* **1993**, *26*, 6455.

MA011875G